

# Hand Pose Estimation via Multiview Collaborative Self-Supervised Learning

Xiaozheng Zheng<sup>1,2</sup>, Chao Wen<sup>2</sup>, Zhou Xue<sup>2</sup>, and Jingyu Wang<sup>1</sup>

<sup>1</sup> State Key Laboratory of Networking and Switching Technology,  
Beijing University of Posts and Telecommunications <sup>2</sup> Pico IDL, ByteDance

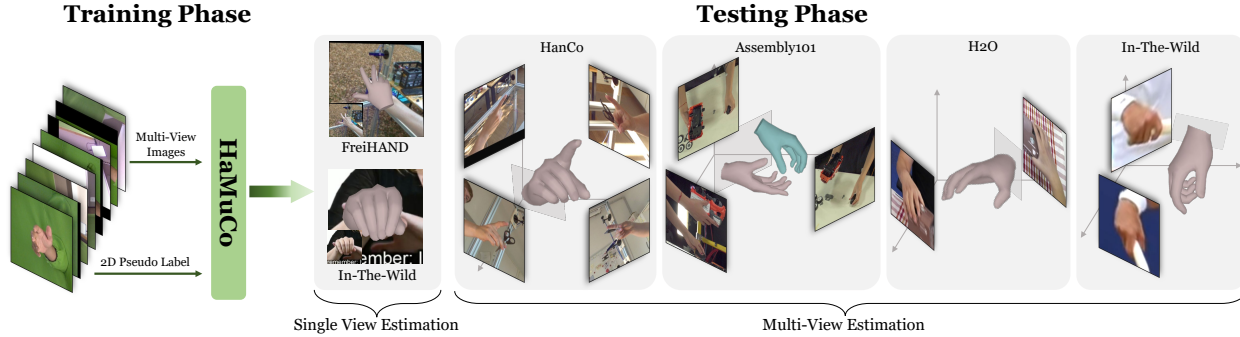


Figure 1. Our method takes multi-view images with 2D pseudo labels for training. From the results on public datasets [37, 54, 72, 74] and in-the-wild images, we demonstrate that our method can estimate accurate 3D hand pose with single- or arbitrary multi-view images.

## Abstract

3D hand pose estimation has made significant progress in recent years. However, the improvement is highly dependent on the emergence of large-scale annotated datasets. To alleviate the label-hungry limitation, we propose a multi-view collaborative self-supervised learning framework, HaMuCo, that estimates hand pose only with pseudo labels for training. We use a two-stage strategy to tackle the noisy label challenge and the multi-view “groupthink” problem. In the first stage, we estimate the 3D hand poses for each view independently. In the second stage, we employ a cross-view interaction network to capture the cross-view correlated features and use multi-view consistency loss to achieve collaborative learning among views. To further enhance the collaboration between single-view and multi-view, we fuse the results of all views to supervise the single-view network. To summarize, we introduce collaborative learning in two folds, the cross-view level and the multi-to single-view level. Extensive experiments show that our method can achieve state-of-the-art performance on multi-view self-supervised hand pose estimation. Moreover, ablation studies verify the effectiveness of each component. Results on multiple datasets further demonstrate the generalization ability of our network.

## 1. Introduction

3D hand pose estimation is essential in various application scenarios, from action recognition and sign language translation to AR/VR [25, 26]. Hand pose estimation has achieved a significant improvement in recent years. However, the progress heavily relies on the emergence of many hand pose datasets with accurate 3D annotations. Acquiring labeled datasets is quite time-consuming and laborious, exposing a realistic challenge for deep learning models to learn with limited and noisy data.

Self-supervised learning is an emerging solution to the challenge posed by manual annotation. Though worth exploring, self-supervised pose estimation with RGB hand images is a challenging and relatively unexplored area with only one pioneering method, S<sup>2</sup>HAND [13]. S<sup>2</sup>HAND aims to conduct 3D hand reconstruction from a single RGB image with the noisy off-the-shell 2D hand pose estimation results (OpenPose) for supervision. Unfortunately, S<sup>2</sup>HAND still suffers from a dilemma that the performance is highly restricted by the quality of the pseudo label in a specific view when handling an ill-posed problem.

This observation motivates us to exploit multi-view information to improve self-supervised learning due to complementary multi-view observations can alleviate the ambiguity of pose estimation. There is some literature using multi-view data for self-supervised human body estimation, including EpipolarPose [35] and CanonPose [62]. How-

ever, these approaches only adopt a single-view network to process isolated views, which makes them not feasible for self-supervised hand pose estimation, whose utilized 2D pseudo labels generated by the off-the-shell 2D hand pose estimator are relatively inaccurate. To our knowledge, no previous work discussed the potential of multi-view in self-supervised hand pose estimation. In this paper, we push along this direction via multi-view collaborative learning. As mentioned in [32], naively enforcing multi-view consistency is prone to generate degenerated solutions. At the early training stage, it may be hamstrung by the majority as “the blind lead the blind”. To summarize, there are several challenges seldom addressed by previous methods, (1) noisy pseudo labels, (2) limited information from cluttered observations, and (3) early-stage divergence.

To this end, we propose a novel two-stage strategy to tackle noisy pseudo label and unreliable multi-view “group-think” issues. Formally, we name the pipeline HaMuCo, which stands for Hand Multiview Collaborative learning. The core insight is to decouple the initial results from the single-view estimation and the updated predictions after cross-view interaction and fusion. Specifically, HaMuCo has (1) the *single-view stage* and (2) the *multi-view stage*. The *single-view stage* provides initial predictions and visual cues from a simple model-based network with the MANO [53] hand model as the decoder. Using a parametric model provides hand priors to regularize irrational anatomy when guided by noisy pseudo labels. The *multi-view stage* is an essential part of our framework, which conducts cross-view interaction, fusion, and distillation. In this stage, we design a cross-view interaction network consisting of a (1) multi-view graph feature extraction module to gather useful information from all views, a (2) dual-branch cross-view interaction module to capture joint-level dependencies across all views, and a (3) parameters regression module. This network is permutation-equivalence and can work with variable input views. To solve the challenge of updating the pose effectively towards consistent results without early divergence, we introduce multi-view collaborative learning in two folds. On the one hand, we design a dual-branch consistency for cross-view level collaborative learning to guide all the views to learn from each other. On the other hand, we achieve self-distillation by fusing the results of all views into a final prediction and using it to supervise the single-view estimations. This procedure further enhances the collaboration between single-view and multi-view networks.

We conduct comprehensive experiments to demonstrate that HaMuCo is simple, effective, and versatile. Abundant experiments on the HanCo [72] dataset validate the efficacy of each component and analyze our model from different aspects. Meanwhile, our method achieves state-of-the-art performance both in single- and multi-view 3D

hand pose estimation, under multi-view self-supervised settings. As shown in Fig. 1, our model can generalize well to other datasets [37, 74] and in-the-wild images. Furthermore, our method can also obtain plausible self-supervised performance on the Assembly101 [54] dataset.

In summary, our contributions are the following:

- We present the first multi-view self-supervised learning framework for 3D hand pose estimation, which can achieve accurate single- and multi-view estimations without any manual annotations for training.
- We propose a cross-view interaction network and supervise it with dual-branch consistency loss and multi-view distillation loss to achieve collaborative learning at a cross-view level and multi- to single-view level.
- We experimentally validate the efficacy of our method on benchmarks and achieve state-of-the-art performance both in single- and multi-view 3D hand pose estimation under multi-view self-supervised settings.

## 2. Related Work

**Hand Pose Estimation.** Hand pose estimation can be categorized into RGB-based methods [31, 59, 73] and depth-based methods [19, 20, 44], depending on the input modality. In this paper, we focus our attention on RGB-based hand pose estimation. The RGB-based methods can be further divided into three categories, *skeleton-based methods* [5, 17, 31, 39, 46, 47, 58, 59, 65–67, 73], *model-based methods* [1, 2, 4, 13, 68, 69, 74], and *mesh-based methods* [11, 12, 14, 21, 36, 38, 40, 41, 45, 60, 71]. *Skeleton-based methods* regress the hand joints directly. Zimmermann *et al.* [73] introduces a multi-stage network that lifts the regressed 2D joints to 3D ones. Variational autoencoder [34] is employed to learn a cross-modal latent space to achieve better hand pose estimation and disentanglement [59, 66, 67]. Latent 2.5D representation regression is proved more effective than direct coordinates regression for hands by [31], which is also adopted by [18, 39, 58, 71]. There are also many works solving hand pose estimation with two hands interactions [18, 37, 46] and hand-object interactions [2, 17, 37]. Recent *model-based methods* make use of MANO [53], which can incorporate the hand prior and predict the hand mesh simultaneously. Those methods [1, 4, 13, 68, 69] rely on additional supervisions [1, 4, 13, 68, 69] or inputs [4]. In contrast, *mesh-based methods* regress each vertex of the hand mesh directly, which is more accurate but requires large-scale datasets with hand mesh annotations [24, 37, 46, 74]. Most of these methods utilize graph convolutional network (GCN) [11, 12, 14, 21, 36, 60, 71] or transformers [40] or both [38, 41] for regression. I2L-MeshNet [45] regresses each vertex by predicting 1D heatmaps of three axes. Chen *et al.* [7] uses an image-to-image translation network to predict the UV map of the mesh.

Similar to previous works [38, 41], our method also utilizes both transformer and GCN. However, we employ them for cross-view interaction. Besides, we also adopt the model-based paradigm for our self-supervised framework. Nevertheless, we do not adopt complex supervision in the single-view network, since we aim to explore multi-view information to improve the estimation.

**Multi-View 3D Human Pose Estimation.** Multi-view information is widely explored to improve 3D human pose estimation by tackling occlusions and depth-ambiguity in a fully-supervised manner [3, 30, 33, 49–51, 55, 70]. Volume-based methods [33, 49, 50, 61] project 2D features or heatmaps of joints to a 3D space for estimation. Another kind of method [30, 51, 70] utilizes the geometry information to fuse the features in 2D space directly and efficiently. Recently, some works [43, 55] utilize transformers for implicit cross-view fusion without camera extrinsics.

**Label-Efficient Learning.** Label-efficient learning aims to reduce the label requirements of the algorithms. Currently, contrastive learning [8–10, 23, 28] is a popular method to learn image representations without any labels, which is also used for mining the hand features [57, 72]. Many works devote to solving single-view hand pose estimation in a label-efficient manner [1, 4, 5, 11, 13, 47, 58, 65, 69, 73]. Synthetic data is used to avoid manual annotation procedures [11, 47, 73], but may need domain transfer [47]. Weakly-/Semi-supervised learning uses additional loss to reduce 3D label demand. Cai *et al.* [5] takes advantage of depth image as weak supervision. Model-based methods [1, 4, 69] can achieve 3D estimation with only mask loss and 2D joint loss. Spurr *et al.* [58] proposes biomechanical constraints to better leverage data with 2D labels. Yang *et al.* [65] utilizes labeled synthetic and unlabelled real data with perturbation augmentations to achieve semi-supervised learning. Chen *et al.* [13] proposes a self-supervised framework with only 2D noisy labels for training. The performance is limited by using only the single-view information because of the quality of the noisy label. Therefore, we introduce multi-view constraints to boost the self-supervised performance, which is not explored for hand pose estimation before.

Multi-view label-efficient learning is explored in 3D human pose estimation [32, 35, 52, 62]. Rhodin *et al.* [52] trains a semi-supervised network with only a small amount of labeled 3D data and multi-view consistency constraints. Iqbal *et al.* [32] mixes single-view images with 2D labels and unlabelled multi-view images for training. EpiporlarPose [35] triangulates multi-view 2D pseudo labels to 3D for training. CanonPose [62] learns to lift 2D pseudo labels to 3D ones with multi-view consistency constraints. Our goal is the same as [35, 62] that aims at training without any manual label. Nevertheless, previous methods do not work well for hands since the pose of a hand can change drastically over time and different joints may have similar appearances.

## 3. Method

As shown in the left part of Fig. 2, our framework consists of two stages, single-view stage and multi-view stage. The single-view stage mainly conducts single-view estimation, while the multi-view stage consists of cross-view interaction and multi-view fusion.

### 3.1. Single-View Stage

**Overview.** Our framework takes multi-view synchronized hand images  $\mathcal{I} = \{\mathbf{I}_i\}_{i=0}^v$  with  $v$  views as input, each view is an image of  $\mathbf{I}_i \in \mathbb{R}^{3 \times h \times w}$ . All the operations of this stage are conducted on each view. The estimation network for the single-view stage is a model-based network. Using the model-based method will reduce the adverse effects of using poor pseudo labels as supervision by providing hand prior information for regularization.

**Hand model.** We employ MANO [53] as the hand model. The hand mesh can be derived from the MANO layer using parameters  $\beta$  and  $\theta$ , *i.e.*  $M(\beta, \theta)$ .  $\beta \in \mathbb{R}^{10}$  and  $\theta \in \mathbb{R}^{16 \times 3}$  control the shape and pose of the hand respectively. We can use a predefined regressor to obtain the 3D joints from the 3D mesh vertices by  $P = JM$ , where  $J \in \mathbb{R}^{k \times n}$ , where  $n = 778$  and  $k = 21$  are the joints number and vertices number. For more details, we recommend referring to [53].

**Camera model.** Following Boukhayma *et al.* [4], we model the geometry correspondence by the weak-perspective camera model and obtain camera parameters from the network predictions. Given the translation vector  $\mathbf{t}$  and scaling value  $s$ , the 2D coordinates in image plane can be obtained by:  $P_{2D} = \Pi(P) = s\Omega(P) + \mathbf{t}$ , where  $\Omega$  is the orthographic projection and  $\Pi$  denotes the weak-perspective projection.

**Network Structure.** Our framework is agnostic to the single-view estimation network. For the sake of simplicity, we employ a CNN as the encoder  $F_e$ , and an MLP as the decoder  $F_d$  for regressing the MANO parameters. We have 3D hand mesh:  $M_i(\theta_i, \beta_i) = F_s(\mathbf{I}_i) = F_d(F_e(\mathbf{I}_i))$ , where  $F_s$  denotes the entire single-view network.

### 3.2. Multi-View Stage

In this section, we introduce the multi-view stage, which is the core of our system to enable the network to exploit multi-view information. This stage conducts cross-view interaction, fusion, and distillation. The critical components of this stage are a cross-view interaction network for capturing cross-view features and several consistent losses for guiding collaborative learning.

#### 3.2.1 Cross-View Interaction Network

**Multi-view graph feature extraction module.** The first step for interaction is to extract the appropriate features. Different from [11, 12, 71], this module collects useful information from multiple views into a graph. Specifically,

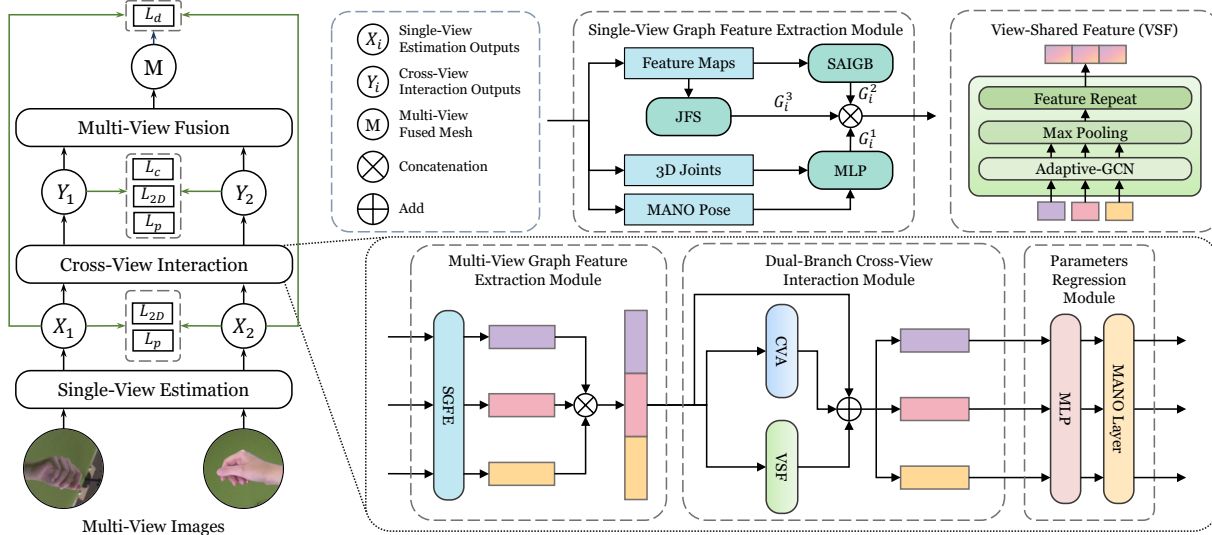


Figure 2. The left illustrates our whole pipeline (2 views for simplicity). The bottom right depicts our cross-view interaction networks (3 views for simplicity). The top right shows the single-view graph feature extraction (SGFE) module and view-shared feature (VSF) module.

it makes use of multi-view feature maps of different levels  $\mathcal{H} = \{\mathbf{H}_i^j\}_{i=0}^v$  (where  $\mathbf{H}_i^j$  is the intermediate feature of encoder after  $j$  residual blocks,  $j=1, 2, 3, 4$ ), 3D joints  $\mathcal{P} = \{\mathbf{P}_i\}_{i=0}^v$ , and MANO pose parameters  $\Theta = \{\theta_i\}_{i=0}^v$  from the single-view stage to extract a multi-view graph feature  $\mathbf{G}$ . The graph feature of each view  $\mathbf{G}_i$  consists of three parts. The first part is joint location embedding  $\mathbf{G}_i^1 \in \mathbb{R}^{k \times c_1}$ , providing the explicit geometric information. This embedding is obtained by using an MLP to map the single-view 3D joints locations  $\mathbf{P}_i$  and pose parameters  $\theta_i$  to dimension  $c_1$ . The second part is joint-wise high-level image features  $\mathbf{G}_i^2 \in \mathbb{R}^{k \times c_2}$  generated by spatial-aware initial graph building (SAIGB) [71] module using the last level feature maps  $\mathbf{H}_i^4$ . This part provides compact image clues of all views for interaction. Inspired by [63, 64], the third part is joint-aligned features  $\mathbf{G}_i^3 \in \mathbb{R}^{k \times c_3}$  gathered by joint feature sampler (JFS). JFS projects joints onto multi-scale feature maps  $\{\mathbf{H}_i^j\}_{j=1}^3$  to retrieve fine-grained features for better local alignment. After that, we concatenate all parts to get view-specific graph feature  $\mathbf{G}_i = [\mathbf{G}_i^1 \otimes \mathbf{G}_i^2 \otimes \mathbf{G}_i^3]$ . Finally, we stack  $\{\mathbf{G}_i\}_{i=0}^v$  of all views to obtain multi-view graph feature  $\mathbf{G} \in \mathbb{R}^{v \times k \times (c_1 + c_2 + c_3)}$ .

**Dual-branch cross-view interaction module.** We design a network to effectively capture complementary information from other views on multi-view graph feature  $\mathbf{G}$ . The interaction module has two branches, (1) *cross-view attention branch* (CVA) and (2) *view-shared feature branch* (VSF). *Cross-view attention branch* utilizes a cross-view transformer  $F_t$  consisting of several multi-head attention layers with token size  $vk$  and MLPs, which allows each joint to aggregate features from other joints or views. This branch implicitly captures the multi-view information. An explicit multi-view prior information is that the observed

poses from all the views should be consistent in 3D. Therefore, we add a branch to excavate the multi-view shared information to enhance the feature representation. Specifically, *view-shared feature branch* first employs adaptive-GCN [17]  $F_a$  to map the view-specific features  $\mathbf{G}_i$  to a canonical feature space  $\mathbf{C}_i = F_a(\mathbf{G}_i)$ . Then, we stack  $\mathcal{C} = \{\mathbf{C}_i\}_{i=0}^v$  together to get multi-view canonical features  $\mathbf{C} \in \mathbb{R}^{v \times k \times (c_1 + c_2 + c_3)}$ . After that, we use max-pooling on  $\mathbf{C}$  to get the max activated features of every joint then repeat them in the view dimension as the view-shared features  $\mathbf{C}' \in \mathbb{R}^{v \times k \times (c_1 + c_2 + c_3)}$ . We denote the dual-branch cross-view interaction as:  $\mathbf{G}^* = \mathbf{G} + F_t(\mathbf{G}) + \mathbf{C}'$ , where  $\mathbf{G}^*$  is the updated graph feature.

**Parameters regression module.** After interaction, we employ a view-shared MLP  $F_r$  to regress the MANO pose parameters  $\theta_i^* = F_r(\mathbf{G}_i^*)$  to derive the hand mesh of each view  $\mathbf{M}_i^*(\theta_i^*, \beta_i)$  and corresponding joints  $\mathbf{P}_i^* = \mathbf{J}\mathbf{M}_i^*$ .

### 3.2.2 Multi-View Collaborative Learning

To allow all the views and the networks to learn collaboratively, we utilize dual-branch consistency loss  $L_c$  upon interaction outputs and distillation loss  $L_d$  between multi-view fusion results and single-view outputs.  $L_c$  introduces collaborative learning between multiple views, guiding the poses from different views to be as close as possible. While  $L_d$  makes the multi-view and single-view stage work in a collaborative manner, introducing a positive cycle between them and achieving a self-boosting effect.

**Multi-view fusion.** Since the refined hand mesh  $\mathbf{M}_i^*$  of every single view should have a consistent pose, we fuse all predictions into a more plausible result  $\hat{\mathbf{M}}$ . Here, we use Procrustes analysis to align meshes to a canonical view. When the camera extrinsics are known, we use relative ro-

**Algorithm 1**  $L_c$  Pseudocode, PyTorch-like

```

def L_c(meshes, batch_idx):
    loss_list, v = [], len(meshes) # view number
    for m1 in meshes:
        aligned_meshes = []
        for m2 in meshes:
            aligned_meshes.append(align(m2, m1))
        fused_mesh = sum(aligned_meshes) / v
        if batch_idx % 2: # update L_c_2D
            L_c_2D = []
            for m2 in aligned_meshes:
                L_c_2D.append(D(m1[:, :2], m2[:, :2]))
            loss_list.append(sum(L_c_2D) / v)
        else: # update L_c_f
            L_c_f = D(fused_mesh, m1)
            loss_list.append(L_c_f)
    return sum(loss_list) / v

def D(a, b): return abs(a.detach() - b).mean()

```

tation to replace the computed relative rotation. Considering the lack of explicit guidance, we empirically introduce a prior that all the views contribute equally. Thus, we simply average all the aligned meshes from different views, *i.e.*  $\tilde{M} = \frac{1}{v} \sum_{i=1}^v A(\mathbf{M}_i^*)$ , where  $A$  denotes align procedure.

**Dual-branch consistency loss.**  $L_c$  consists of *multi-view 2D consistency loss*  $L_{c_{2D}}$  and *multi-view fusion consistency loss*  $L_{c_f}$ . The motivation behind  $L_{c_{2D}}$  is that the 2D predictions in the x-axis and y-axis are more accurate than the depth prediction in the z-axis. Therefore,  $L_{c_{2D}}$  utilizes the 2D predictions in every single view as the pseudo label to supervise other views, which explores the view-specific reliable information to collaboratively improve the predictions of all the views. *Multi-view 2D consistency loss* is defined as:  $L_{c_{2D}} = \frac{1}{v^2} \sum_{i=1}^v \sum_{j=1}^v \|\Pi(\mathbf{M}_i^*) - \Pi(A_i(\mathbf{M}_j^*))\|_1$ , where  $A_i(\cdot)$  denotes the alignment operation to align a specific view to  $i^{th}$  view. *Multi-view fusion loss* uses the multi-view fusion results to supervise each view on account of the fusion results being more plausible under most situations. The loss is defined as:  $L_{c_f} = \frac{1}{v} \sum_{i=1}^v \|\mathbf{M}_i^* - A_i^{-1}(\tilde{M})\|_1$ , where  $A_i^{-1}(\cdot)$  denotes the inverse transformation from canonical view to  $i^{th}$  view.  $L_{c_{2D}}$  and  $L_{c_f}$  are complementary to each other. Only using  $L_{c_{2D}}$  tends to get performance saturation faster. In contrast, only adopting  $L_{c_f}$  can lead to unstable training since there may exist the situation that the fusion results are worse due to the majority of the predictions being wrong, especially at the early training stage. During training, we alternately update  $L_{c_{2D}}$  and  $L_{c_f}$  to achieve more stable and better optimization. The pseudocode of  $L_c$  is in Algorithm 1.

**Multi-view distillation loss.** Since the multi-view fusion results are much better than the 2D pseudo label, we introduce multi-view distillation loss  $L_d = \frac{1}{v} \sum_{i=1}^v \|\mathbf{M}_i - A_i^{-1}(\tilde{M})\|_1$  that uses the fusion results to supervise the single-view outputs to achieve self-distillation.

**Total loss.** Except for the losses for multi-view collaborative learning, our framework also adopts two general losses,




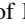
Method	Input	N-JE↓	PA-JE↓
<i>Fully-Supervised Method:</i>			
MobRecon [11]	image	9.9	5.7
EpipolarPose [35]	image	10.5	6.1
<i>Self-Supervised Method:</i>			
EpipolarPose [35]	image, 	19.7	9.3
CanonPose [62]	2D pose, 	31.9	13.0
<b>Ours</b>	<b>image, </b>	<b>11.1</b>	<b>7.0</b>
EpipolarPose [35]	image	42.3	23.5
CanonPose [62]	2D pose	32.8	13.2
<b>Ours</b>	<b>image</b>	<b>15.2</b>	<b>7.7</b>

Table 1. Comparisons of single-view inference performance with other methods on the testing split of HanCo dataset.  denotes the method that needs camera extrinsics for training.

2D joints loss, and model prior loss. The final loss is defined as:

$$L = L_{2D} + \alpha L_p + L_c + L_d, \quad (1)$$

where  $L_{2D} = \frac{1}{v} \sum_{i=1}^v w_i (\|\mathbf{P}_i^* - \hat{\mathbf{P}}_i\|_1 + \|\mathbf{P}_i - \hat{\mathbf{P}}_i\|_1)$ ,  $L_p = \frac{1}{v} \sum_{i=1}^v (\|\boldsymbol{\theta}_i\|_1 + \|\boldsymbol{\theta}_i^*\|_1 + \gamma \|\boldsymbol{\beta}_i\|_1)$ ,  $\hat{\mathbf{P}}_i$  denotes pseudo 2D joint label with confidence  $w_i$  of  $i^{th}$  view from OpenPose [6], and  $\alpha$  and  $\gamma$  are used to balance the loss scale.

## 4. Experiments

### 4.1. Datasets and Metrics

**FreiHAND** [74] is a dataset for single-view 3D hand pose estimation, which contains 130,240 training images and 3,960 testing images. All images are captured from the real world with 3D annotations. The training set consists of 32,560 composited images with four types of real-world backgrounds and hands captured against a green screen.

**HanCo** [72] extends FreiHAND, which consists of 1,517 videos with multiple views and camera calibration. It has 860,304 frames in total, *i.e.* 107,538 time-step per view. Since HanCo does not have an official train/test split, we use the first 1,200 sequences for training and the last 317 sequences for testing in all experiments for fair comparisons. We use images recorded against a green screen as the training set. To enhance the background variety of the testing set, we do not include green screen images for it. Therefore, it is more challenging for testing.

**Other datasets.** We also provide additional qualitative results on other datasets. Assembly101 [54] is an action recognition dataset that consists of 4,321 videos sequence. H2O [37] is a hand-object interaction dataset with 571,645 frames. Please refer to supplementary materials for details.

**Metrics.** We report standard metrics for hand pose estimation as follows. (1) **MPJPE/MPVPE** (mean per joint/vertex position error) measures the average Euclidean distance

Method	Train set	Backbone	PA-JE↓	PA-VE↓	F@5↑	F@15↑
<i>Fully-Supervised Method:</i>						
YoutubeHand [36]	FreiHAND	Res50	8.4	8.6	0.61	0.97
I2L-MeshNet [45]	FreiHAND	Res50 <sup>†</sup>	7.4	7.6	0.68	0.97
METRO [40]	FreiHAND	HRNet	6.7	6.8	0.72	0.98
Tang <i>et al.</i> [60]	FreiHAND	Res50	6.7	6.7	0.72	0.98
I2UV-HandNet [7]	FreiHAND	Res50	6.7	6.9	0.71	0.98
MobRecon [11]	FreiHAND	Res50 <sup>†</sup>	6.1	6.2	0.76	0.98
<i>Weakly-Supervised Method:</i>						
S <sup>2</sup> HAND [13]	FreiHAND	EffiNet-b0	/	/	0.42	0.89
Ours*	FreiHAND	Res50	9.8	9.9	0.55	0.95
<i>Self-Supervised Method:</i>						
S <sup>2</sup> HAND [13]	FreiHAND	EffiNet-b0	11.8	11.9	0.48	0.92
Ours*	FreiHAND	Res50	11.9	12.0	0.47	0.92
Ours*	HanCo	Res50	11.6	11.8	0.48	0.93
Ours	HanCo	Res50	6.2	6.7	0.72	0.99

Table 2. Performance comparisons on the FreiHAND evaluation set. <sup>†</sup> denotes using a stacked backbone structure and \* means only using our single-view network for training.

in mm between the predicted and ground-truth joints/vertices. JE/VE are the abbreviations for MPJPE/MPVPE. (2) **NMPJPE/NMPVPE** (normalized mean per joint/vertex position error, N-JE/VE) computes MPJPE/MPVPE after performing translation and scale alignment. (3) **PA-MPJPE/PA-MPVPE** (PA-JE/VE) is a modification of MPJPE/MPVPE with Procrustes analysis [22]. This metric normalizes the absolute scale, center, and rotation. (4) **F-Score** [13] is the harmonic mean of recall and precision between two meshes w.r.t. a specific distance threshold. F@5mm and F@15mm are reported. (5) **AUC** means the area under the curve of the PCK, where the PCK refers to the percentage of correct joints.

## 4.2. Implementation Details

We implement all the networks in PyTorch [48]. We use a pretrained [15] ResNet [29] as backbone. We first train our framework without multi-view consistency loss and distillation loss for 10 epochs. Then, we finetune the whole framework for 30 epochs. Each batch contains images from 8 time-step of 8 cameras. We use AdamW [42] as the optimizer. We start training with an initial learning rate of  $3e-4$  and use the cosine decay schedule. We crop the hands from the input images and resize them to  $256 \times 256$ . We adopt color transformation, translation, rotation, and scaling as training augmentation. Please refer to supplementary materials for more details.

## 4.3. Comparisons with state-of-the-arts

Since HaMuCo can conduct single- and multi-view inference, we compare our method with other competitors under various settings.

Method	MPJPE ↓	PA-MPJPE ↓
<i>Fully-Supervised Method:</i>		
Algebraic [33]	5.5	3.6
Volumetric [33]	5.8	3.6
Volumetric* [33]	<b>4.9</b>	3.6
Ours (Opt-Center)	6.0	<b>3.2</b>
<i>Triangulation Method (without training):</i>		
DLT [27]	16.8	13.2
Pictorial [16]	13.5	10.2
RANSAC [33]	12.3	9.8
<i>Self-Supervised Method:</i>		
Algebraic [33]	10.3	7.8
Volumetric [33]	10.6	8.0
Volumetric* [33]	9.5	7.2
Ours (Opt-Center)	8.8	<b>5.3</b>
Ours (RANSAC)	<b>8.5</b>	5.6

Table 3. Multi-view inference comparisons on the HanCo dataset. The notation \* indicates using the ground-truth 3D center.

### 4.3.1 Single-View Inference

On HanCo, we compare with EpipolarPose [30] and CanonPose [62] under the multi-view self-supervised training setting with/without camera extrinsics. On FreiHAND, we compare with S<sup>2</sup>HAND [13] under the single-view weakly-/self-supervised setting. Moreover, we compare our self-supervised performance with recent fully-supervised state-of-the-art methods [7, 11, 35, 36, 40, 45, 60] on both datasets. **Hanco.** Since there are no related works reporting performance on HanCo, we implement EpipolarPose, CanonPose, and MobRecon, using their open-source code. As shown in Tab. 1, when camera extrinsics are available, CanonPose performs the worst because it lifts poor 2D predictions from OpenPose (its error is shown in Fig. 4) to 3D ones. EpipolarPose gets a much better performance than CanonPose. In contrast, our method outperforms both of them by a large margin. Without camera extrinsics, our performance is still much better. This indicates the importance of introducing a cross-view interaction network with multi-view constraints and training in a self-boosting loop. Furthermore, our self-supervised performance can get comparable to fully-supervised MobRecon and EpipolarPose.

**FreiHAND.** The comparisons on the evaluation set are shown in Tab. 2. When conducting single-view training on FreiHAND, our self-supervised performance is similar to S<sup>2</sup>HAND, and weakly-supervised performance is better than it. When conducting multi-view training on HanCo, our self-supervised performance can get comparable to or even better than the fully-supervised performance of other methods, even though we employ a simple single-view network. It is worth mentioning that our performance using single-view for training on the FreiHAND and HanCo datasets is similar, which means our performance is not highly related to the difference in the training set.

ID	Method	NMPJPE ↓			PA-MPJPE ↓		
		Single	Interact	Fusion	Single	Interact	Fusion
<i>ResNet-50 as the backbone:</i>							
1	Full	<b>11.14</b> <sub>↑0.03</sub>	8.31 <sub>↓0.03</sub>	<b>7.65</b> <sub>↑0.10</sub>	<b>7.05</b> <sub>↑0.17</sub>	<b>5.35</b> <sub>↑0.07</sub>	<b>5.34</b> <sub>↑0.06</sub>
<i>ResNet-18 as the backbone:</i>							
2	Full	11.17	<b>8.28</b>	7.75	7.22	5.42	5.40
3	- VSF	11.21 <sub>↓0.04</sub>	8.49 <sub>↓0.21</sub>	7.81 <sub>↓0.06</sub>	7.25 <sub>↓0.03</sub>	5.52 <sub>↓0.10</sub>	5.50 <sub>↓0.10</sub>
4	- CVA	11.31 <sub>↓0.14</sub>	8.45 <sub>↓0.17</sub>	7.81 <sub>↓0.06</sub>	7.29 <sub>↓0.07</sub>	5.48 <sub>↓0.06</sub>	5.46 <sub>↓0.06</sub>
5	- $G^1$	11.31 <sub>↓0.14</sub>	8.56 <sub>↓0.28</sub>	7.77 <sub>↓0.03</sub>	7.31 <sub>↓0.09</sub>	5.52 <sub>↓0.10</sub>	5.49 <sub>↓0.09</sub>
6	- $G^2$	11.33 <sub>↓0.16</sub>	8.38 <sub>↓0.10</sub>	7.83 <sub>↓0.08</sub>	7.34 <sub>↓0.08</sub>	5.45 <sub>↓0.03</sub>	5.42 <sub>↓0.02</sub>
7	- $G^3$	11.30 <sub>↓0.13</sub>	8.99 <sub>↓0.69</sub>	7.82 <sub>↓0.07</sub>	7.30 <sub>↓0.08</sub>	5.45 <sub>↓0.03</sub>	5.44 <sub>↓0.04</sub>
8	- $L_{e2D}$	11.25 <sub>↓0.08</sub>	8.43 <sub>↓0.15</sub>	7.90 <sub>↓0.15</sub>	7.32 <sub>↓0.10</sub>	5.58 <sub>↓0.16</sub>	5.57 <sub>↓0.17</sub>
9	- $L_{e_f}$	11.74 <sub>↓0.57</sub>	8.98 <sub>↓0.70</sub>	8.38 <sub>↓0.63</sub>	7.55 <sub>↓0.33</sub>	5.84 <sub>↓0.42</sub>	5.80 <sub>↓0.40</sub>
10	- CVI	13.52 <sub>↓2.35</sub>	/	11.99 <sub>↓4.24</sub>	9.59 <sub>↓2.37</sub>	/	9.42 <sub>↓4.02</sub>
11	- $L_c$	14.04 <sub>↓2.87</sub>	17.03 <sub>↓8.75</sub>	10.32 <sub>↓2.57</sub>	9.04 <sub>↓1.82</sub>	10.21 <sub>↓4.79</sub>	7.92 <sub>↓2.52</sub>
12	- $L_d$	17.05 <sub>↓5.88</sub>	8.56 <sub>↓0.28</sub>	8.01 <sub>↓0.26</sub>	10.13 <sub>↓2.91</sub>	5.67 <sub>↓0.25</sub>	5.65 <sub>↓0.25</sub>

Table 4. Quantitative ablation studies. We remove each of our components here to show their contribution to our framework. Full denotes our complete model. CVI represents our whole cross-view interaction network. Other notations are consistent with Sec. 3. We report the errors of single-view outputs (Single), cross-view interaction outputs (Interact), and multi-view fusion results (Fusion).

### 4.3.2 Multi-View Inference

Since our method employs a multi-view network, we compare our multi-view inference performance with other competitors under different settings on the HanCo testing set in Tab. 3. A simple solution for multi-view inference is triangulation without any training. We show the performance of some triangulation methods. Using Direct Linear Transform (DLT) [27] gets inferior performance due to the noise in some views. Using pictorial structure [16] to exploit the bone prior and joint uncertainty can significantly improve the performance. RANSAC implemented by [33] can get better performance because it can reject outliers.

Considering there are no other self-supervised methods conducting multi-view inference, we implement a fully-supervised multi-view 3D human pose estimation method [33] in a self-supervised manner. Specifically, we use the RANSAC outputs as the pseudo label to train their two models (Algebraic and Volumetric). Algebraic model [33] incorporating learnable confidence of different views into triangulation predicts better than triangulation. Volumetric model [33] projecting 2D features into 3D volume for inference obtains results better than the pseudo label, but the performance is related to the accuracy of the hand center.

However, both of these two models are inferior to ours. As our method predicts the root-relative 3D pose, we should conduct some postprocessing to obtain the absolute world coordinates. We introduce two different ways to achieve it, 1) using the 2D predictions of different views to triangulate and refine a center for our root-relative results and 2) conducting RANSAC triangulation using our 2D predictions. Both of these two methods have their merits. Obtaining the

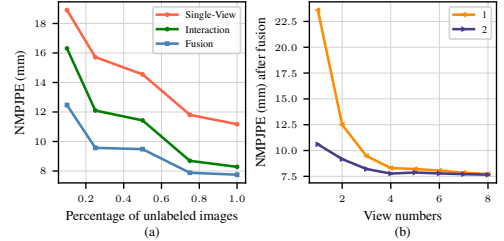


Figure 3. Error of using different (a) #training data, (b) (line-1)#view for training, and (line-2)#view for inference when trained with 8 views.

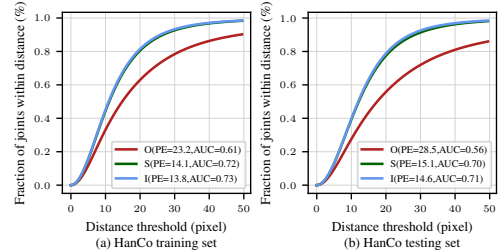


Figure 4. AUC of three 2D joint sets. O, S, I, PE denote OpenPose, single-view, interaction, and average pixel error in resolution  $256 \times 256$ .

center can keep the root-relative results with hand prior, resulting in low PA-MPJPE. In contrast, RANSAC gets better joint-wise accuracy, which is indicated by low MPJPE.

We also compare our method with the fully-supervised version of [33]. The comparison reveals that there is still a multi-view inference performance gap between our self-supervised method and the fully-supervised method [33], which can be filled by future works. Nonetheless, our method can achieve comparable fully-supervised performance, showing the versatility of our method.

### 4.4. Ablation Study

We conduct comprehensive ablation experiments on the HanCo [72] dataset to show the effectiveness of each component. All results are shown in Tab. 4.

**Different backbones.** We first show our performance with different backbones. As shown in #1 and #2, using a large backbone like Res50, our performance can be further improved. For efficiency, we conduct ablation studies using Res18 as the backbone unless otherwise specified.

**Two branches for cross-view interaction module.** As presented in #3 and #4, both of the branches can reduce the error. VSF can explicitly model the view-shared information and add reliable information from every view. CVA can capture the self-/cross-view joint-level correlations.

**Graph features.** The results indicate that three kinds of features (#5, #6, #7) all lead to performance improvement. Especially, local feature (#7,  $G^3$ ) can notably reduce the error after the interaction by providing fine-grained details.

**Cross-view interaction network (CVI).** We also conduct experiments to show the importance of CVI by removing

it and posing consistency constraints in single-view outputs like [32]. In this way, the performance drops dramatically (#10), proving the necessity of using CVI to capture the features of all the views for self-supervised learning.

**Two branches for multi-view consistency loss.** Without enforcing cross-view interaction outputs to be consistent, the performance significantly drops (#9). If we do not explore relatively more reliable 2D predictions to enhance consistency, the performance can also get worse (#8).

**Dual-branch consistency loss.** The performance is unsatisfactory (#11) when employing the cross-view interaction network without any consistency constraints (*i.e.* discard #8 and #9). The interaction network should cooperate with consistency so that the constraints can guide the network to exploit multi-view information to function better.

**Multi-view distillation loss.** Removing the multi-view distillation loss, all the metrics drop by a large margin (#12), especially in single-view estimation accuracy. This phenomenon proves the effectiveness of collaborative learning between single- and multi-view networks.

#### 4.5. Model Analysis

**Postprocessings for world coordinates.** As discussed in Sec. 4.3.2, our method needs postprocessing to obtain the absolute coordinates. Directly using the 2D center for triangulation performs the worst due to the error accumulation (JE:9.51mm, PA-JE:5.34mm). Optimizing a 3D pose with 2D predictions ignores the hand prior provided by MANO, resulting in a significant PA-JE drop (JE:8.79mm, PA-JE:5.88mm). Both optimizing a center and using RANSAC triangulation can get good results, as discussed in Sec. 4.3.2.

**Different percentage of unlabeled images.** Fig. 3 (a) shows our method can get consistent performance improvement as the unlabeled training data increases.

**Different view number for training.** The **line-1** in Fig. 3 (b) shows the performance of our method tested on a certain view when trained with different view numbers. The curve shows that our method can be consistently improved as the number of views increases. We also observe that using multiple views for training can significantly improve performance when the valid views are few.

**Different view number for inference.** Our model allows inferring with an arbitrary number of views. However, when the model is trained with a fixed view number, it could get the view number bias, resulting in better performance using the view number close to the training one. To avoid this, we add random masks in our interaction module and finetune the model for a few epochs. After that, results can get better by a small margin (single-view error is 11.07mm and fusion error 7.60mm, both in NMPJPE.). The **line-2** in Fig. 3 (b) shows results on a certain view when trained on 8 views and tested on 1 to 8 views. We can observe consistent improvement with the inference view number increases.

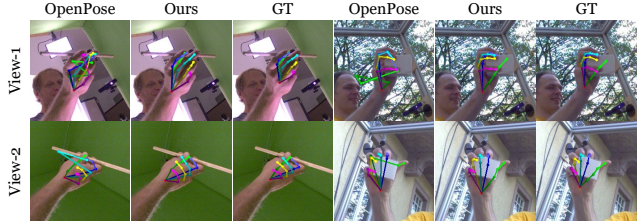


Figure 5. 2D prediction (overlayed in the images) comparisons between OpenPose, ours, and ground-truth on the HanCo dataset.

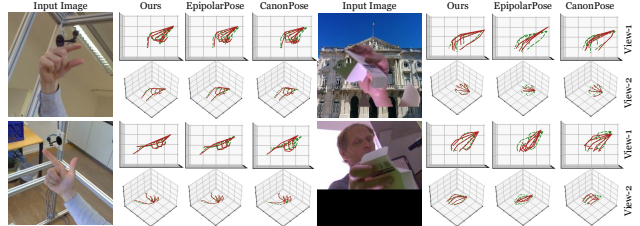


Figure 6. 3D prediction comparisons between our method, EpipolarPose, and CanonPose on the HanCo dataset. Our prediction and ground-truth are shown in solid red and dashed green respectively.

**Different 2D joint sets.** Fig. 4 presents the accuracy of different 2D joint sets on the HanCo training and testing set. Our 2D predictions are extremely better than OpenPose 2D pseudo label used for training.

#### 4.6. Qualitative Result

Fig. 9 presents the visual comparisons of 2 views between 2D joints of OpenPose, ours, and ground-truth on the HanCo dataset. We can observe that our method is more robust for outliers and can generate predictions close to the labels. Fig. 10 shows the 3D predictions from two viewpoints of ours, EpipolarPose, and CanonPose on the HanCo dataset. The results indicate that our method can get more accurate results especially when the occlusions are severe.

### 5. Conclusion

In this paper, we present the first attempt to achieve 3D hand pose estimation via multi-view collaborative self-supervised learning. We adopt a two-stage framework with a cross-view interaction network to capture cross-view dependencies and several novel losses to guide collaborative learning at cross-view and multi- to single-view levels. When only using the multi-view noisy 2D label for training, our model achieves state-of-the-art performance on single- and multi-view hand pose estimation and reasonable generalization to in-the-wild images. The major limitation of our method is that we make an assumption that all the views contribute equally. Mining the most reliable information in every view for fusion remains untouched by our work, which may bridge the gap between the self- and fully-supervised multi-view estimation performance.



## Supplementary Materials

In the supplemental material, we provide:

- §A Implementation Details.
- §B More Experiments and Results.
- §C Video Demo.

### A. Implementation Details

#### A.1. Single-View Network

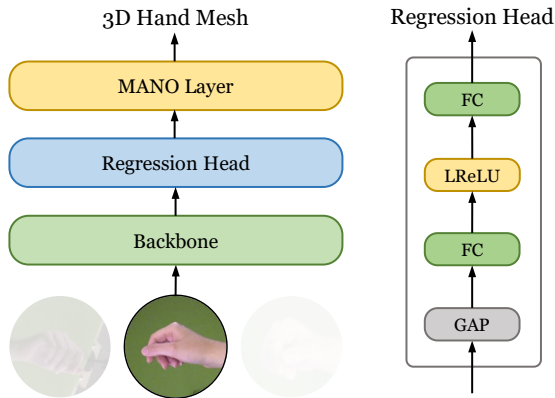


Figure 7. The details of our single-view estimation network.

As described in our paper, we only adopt a simple single-view estimation network for our framework. The details of our single-view network are shown in Fig. 7. The network only consists of a backbone (ResNet [29]) for image feature extraction, a regression head for regressing the MANO [53] parameters, and a MANO layer for parameters decoding to obtain hand mesh. Besides, the regression head is quite simple, only stacking 1 global average pooling (GAP) layer, 2 fully-connected layers, and 1 Leaky-ReLU layer.

#### A.2. Multi-View Graph Feature Extraction Module

Here, we will provide more details about our multi-view graph feature extraction module. The multi-view graph extraction conducts single-view graph extraction (SGFE) for each view at first. SGFE consists of three view-shared modules, a location embedding (LE) module, a spatial-aware initial graph building (SAIGB) module [71], and a joint feature sampler (JFS). LE uses an MLP to map the predicted 3D joints  $P_i \in \mathbb{R}^{21 \times 3}$  and MANO pose parameters (without root joint)  $\theta'_i \in \mathbb{R}^{15 \times 3}$  from the single-view estimation network to the joints embeddings  $G_i^1 \in \mathbb{R}^{21 \times 64}$ . SAIGB

first uses an MLP to scale the channel number of the high-level feature maps  $H_i^4 \in \mathbb{R}^{2048 \times 8 \times 8}$  to a dimension  $21 \times 8$ . Then, it reshapes the features to obtain  $G_i^2 \in \mathbb{R}^{21 \times 512}$ . Motivated by [63, 64], we design a joint feature sampler (JFS) to sample the joint-aligned features from the middle-level feature maps. The details of our JFS are shown in Fig. 8. Given the 3D coordinates of hand joints, we calculate its 2D projections on the feature map using weak perspective projection, then gather the features from nearby pixels via bilinear interpolation. In particular, we sample the joint-aligned features from three levels of the feature maps  $\{H_i^j\}_{j=1}^3$  to obtain  $G_i^3 \in \mathbb{R}^{21 \times 1792}$ . After concatenation and stack, we obtain multi-view graph feature  $G \in \mathbb{R}^{21 \times 2368}$ .

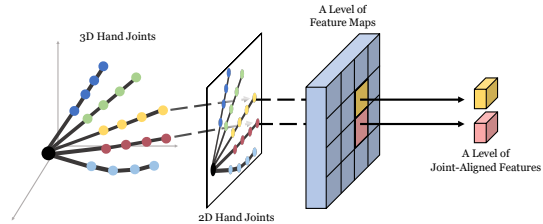


Figure 8. Illustration of our joint feature sampler (JFS) sampling a level of the joint-aligned features for 2 joints.

#### A.3. Architecture Details

Tab. 5 shows the details of our complete architecture. Unless otherwise specified, MLP denotes using 2 fully-connected layers and 1 Leaky-ReLU layer (same as the regression head in Fig. 7 without GAP). We use 2 layers of CVA and VSF in the dual-branch cross-view interaction module (e.g. CVA-1 denotes the first CVA branch). We will release the code after acceptance.

#### A.4. Loss weights

To balance multiple loss functions, we introduce  $\alpha$  and  $\gamma$  in our loss function. For all of our experiments, we set  $\alpha = 0.01$  and  $\gamma = 100$ . It is worth mentioning that adjusting  $\alpha$  to a correct scale is important for self-supervised learning because  $\alpha$  balances the strength of hand-prior information provided by the MANO and the trustworthiness of pseudo labels. When the pseudo labels are reliable, we can reduce  $\alpha$  to trust the pseudo labels more. Otherwise, we should enlarge  $\alpha$  to use MANO to regularize irrational poses.

#Out	#In	Shape	Operation	Notation
<i>Backbone:</i>				
1	/	(8, 3, 256, 256)	Input	$I$
2	1	(8, 64, 64, 64)	ResLayer	
3	2	(8, 256, 64, 64)	ResBlock1	$H^1$
4	3	(8, 512, 32, 32)	ResBlock2	$H^2$
5	4	(8, 1024, 16, 16)	ResBlock3	$H^3$
6	5	(8, 2048, 8, 8)	ResBlock4	$H^4$
<i>Single-View Decoder:</i>				
7	6	(8, 2048)	GAP	
8	7	(8, 48)	MLP	$\theta$
9	7	(8, 10)	MLP	$\beta$
10	7	(8, 3)	MLP	$s, t$
11	8,9	(8, 778, 3)	MANO	$M$
12	11	(8, 21, 3)	Regressor	$P$
<i>Multi-View Graph Feature Extraction:</i>				
13	8,12	(8, 21, 64)	LE	$G^1$
14	6	(8, 21, 512)	SAIGB	$G^2$
15	3,4,5	(8, 21, 1792)	JFS	$G^3$
16	13,14,15	(8, 21, 2368)	Concat	
17	16	(168, 2368)	Reshape	$G$
<i>Dual-Branch Cross-View Interaction:</i>				
18	17	(168, 2368)	CVA-1	
19	17	(168, 2368)	VSF-1	
20	17,18,19	(168, 2368)	Add	
21	20	(168, 2368)	CVA-2	$F_t(G)$
22	20	(168, 2368)	VSF-2	$C'$
23	20,21,22	(168, 2368)	Add	$G^*$
<i>Parameters Regression:</i>				
24	23	(168, 32)	MLP	
25	24	(8, 672)	Reshape	
26	25	(8, 48)	MLP	$\theta^*$
27	25	(8, 3)	MLP	$s^*, t^*$
28	9,26	(8, 778, 3)	MANO	$M^*$
29	28	(8, 21, 3)	Regressor	$P^*$

Table 5. The architecture of our whole network. We show the output shapes after every operation when adopting ResNet-50 as the backbone and taking 8 views of images of resolution  $256 \times 256$  as the input. #Out and #In denotes the output and input index of this operation. In the last column, we specify those outputs that have notations in our paper.

## B. Experiments and Results

### B.1. Datasets

**Assembly101** [54] is an action recognition dataset that consists of 4,321 videos recording different persons manipulating toys. It is recorded by 8 simultaneous static cameras and 4 egocentric cameras. We only use 8 sequences of 8 static cameras for training and present the qualitative results on an additional sequence.

**H2O** [37] provides synchronized multi-view RGB-D images with two hands manipulating objects. The data captured by 4 static cameras and 1 egocentric camera consists

of 344,645 frames for training, 73,380 frames for validation and 153,620 frames for testing. We only evaluate our cross-dataset performance on this dataset using one sequence with 1 egocentric camera and 2 static cameras.

### B.2. Pseudo Labelling

We obtain the 2D joints pseudo labels at an offline stage through an implementation<sup>1</sup> of OpenPose [6, 56]. For HanCo [72], we directly input the images with the original size due to the images having been cropped already. For Assembly101 [54], we use a hand detector to locate and crop the hands. Then, we input the cropped images to obtain the pseudo labels.

### B.3. Model Analysis

**Different view number for training and inference.** Here, we explain the camera settings of the experiments evaluating the performance of our models using different view numbers for training and inference (Fig. 3 in the main submission). Specifically, all the camera settings follow two rules. First, we only test the performance on a specific view for fair comparisons, considering only one specific view is available for all the experimental settings. Second, we choose camera combinations that cover a wider field of vision so that more information can be provided when the camera number has been determined.

**Multi-view weakly-supervised learning.** Our method can also be applied to weakly-supervised learning. Therefore, we conduct an experiment to show the performance of our model using weak 2D supervision. Considering the 2D labels from different views of the HanCo dataset are projected by the same 3D label, using all the 2D labels as weak supervisions may introduce implicit 3D supervision. Therefore, we only utilize the 2D labels from a specific view for weakly-supervised learning. During the training, we set the confidence of the labels to 1. As shown in Tab. 6, when incorporating the label of a view, the performance can be improved. The performance improvement of single-view and interaction without alignments is not significant compared to others. The reason may be two folds. First, it is difficult to obtain a correct rotation from single-view inference. Second, multi-view inference without extrinsics is not able to well correct the global rotation error from every single view. In summary, our method can benefit from available 2D labels, especially when using multi-view images for inference.

### B.4. Additional Qualitative Results

Fig. 9 shows the 2D visual comparisons between OpenPose, our single-view inference results, and the ground-truth. The results demonstrate that OpenPose can obtain

<sup>1</sup><https://github.com/Hzzzone/pytorch-openpose>

NMPJPE ↓			PA-MPJPE ↓		
Single	Interact	Fusion	Single	Interact	Fusion
<i>Self-supervised learning:</i>					
11.17	8.28	7.75	7.22	5.42	5.40
<i>Weakly-supervised learning (one view of the 2D ground-truth is available):</i>					
11.06 <sub>↑0.11</sub>	7.84 <sub>↑0.44</sub>	6.84 <sub>↑0.91</sub>	6.87 <sub>↑0.35</sub>	4.49 <sub>↑0.93</sub>	4.44 <sub>↑0.96</sub>

Table 6. Performance comparisons of our method under self- and weak-supervised settings.

plausible results for those visible joints, which is essential for self-supervised learning. However, the major problem with OpenPose is that it is not robust for invisible joints. When some joints are invisible, it can predict some particularly incorrect results and tend to predict the visible joints as the invisible ones. In contrast, our model-based method with hand prior information obtains a more robust performance towards different kinds of occlusions when the multi-view self-supervised learning provides enough accurate results for supervision.

Fig. 10 provides more visual comparisons between our method, EpipolarPose [35], and CanonPose [62]. All these 3D predictions are obtained with the single-view inference of the models trained by multi-view self-supervised learning. Besides, for better visualization, the predictions in the images are results after alignment with the ground-truth. From the predictions from 2 viewpoints, we can see that our method can obtain more accurate 3D joints with different gestures, backgrounds, viewpoints, occlusions, and objects in hands.

Fig. 11 displays the visualization of our method on the testing sequence of the Assembly101 dataset. We only train a right-hand model, and the left-hand predictions are obtained using the flipped left-hand cropped images for inference. The results demonstrate that our method can be applied to more complicated situations where the available number of hands is unknown at each time step and the occlusions are severe.

Fig. 12 compares our multi-view inference performance with Learnable Triangulation [33] (algebraic version). All the models are trained with self-supervised learning. The predictions are aligned with the ground-truth for better visualization. The results indicate that our method can generate more plausible results with multi-view inference when the camera parameters are available.

Fig. 13 illustrates our cross-dataset predictions on the testing sequence of the H2O dataset. We make use of our model trained on the HanCo dataset to estimate the hand poses with images from multiple uncalibrated cameras. The results demonstrate that our method can generalize to other multi-view settings with unknown camera parameters.

Fig. 14 visualizes the 2D prediction comparisons between S<sup>2</sup>HAND [13], our method, and the ground-truth on

the evaluation set of the FreiHAND dataset [74]. The results of S<sup>2</sup>HAND are obtained by their open-source code<sup>2</sup> with the provided pretrained weights. As shown in the images, our model using multi-view self-supervised learning on the HanCo dataset can obtain plausible single-view predictions on the FreiHAND dataset.

Fig. 15 presents our failure cases on the HanCo dataset. Most of our fails are predictions from samples with challenging viewpoints and severe occlusions. Moreover, the failing predictions mainly fall into two patterns. One is incorrect hand scales and centers, and the other is wrong hand poses. Since the cross-view interaction does not explicitly use the camera extrinsics, it is difficult for it to fix those predictions with incorrect scale and center. However, from those results, we can see that it can solve the incorrect hand poses to some extent.

### C. Video Demo

We provide additional sequential qualitative results in the attached video.

<sup>2</sup><https://github.com/TerenceCYJ/S2HAND>

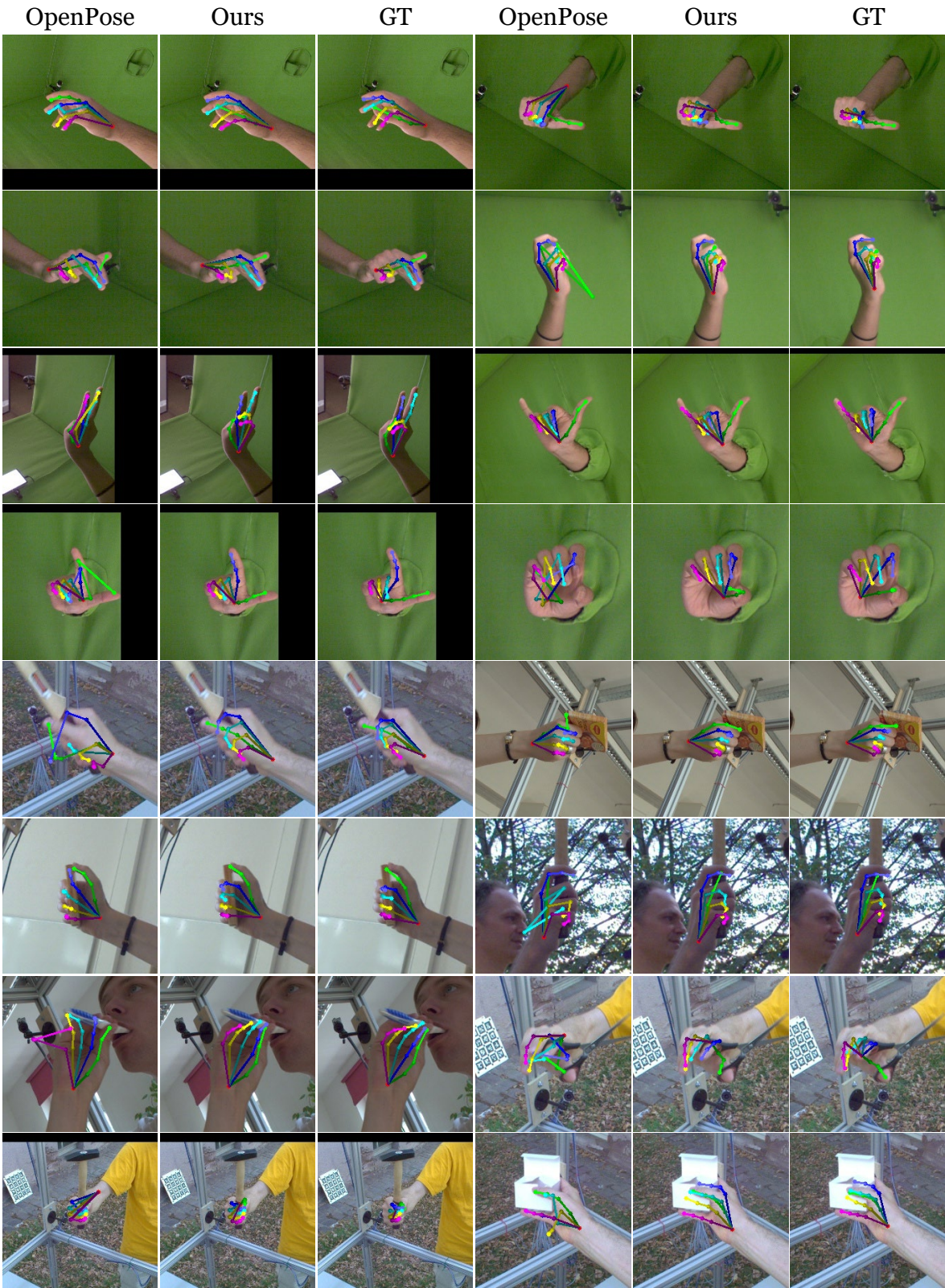


Figure 9. 2D prediction (overlayed in the images) comparisons between OpenPose, ours, and the ground-truth on the HanCo dataset.



Figure 10. 3D prediction comparisons between our method, EpipolarPose, and CanonPose on the HanCo dataset. Our prediction and the ground-truth are shown in solid red and dashed green respectively.

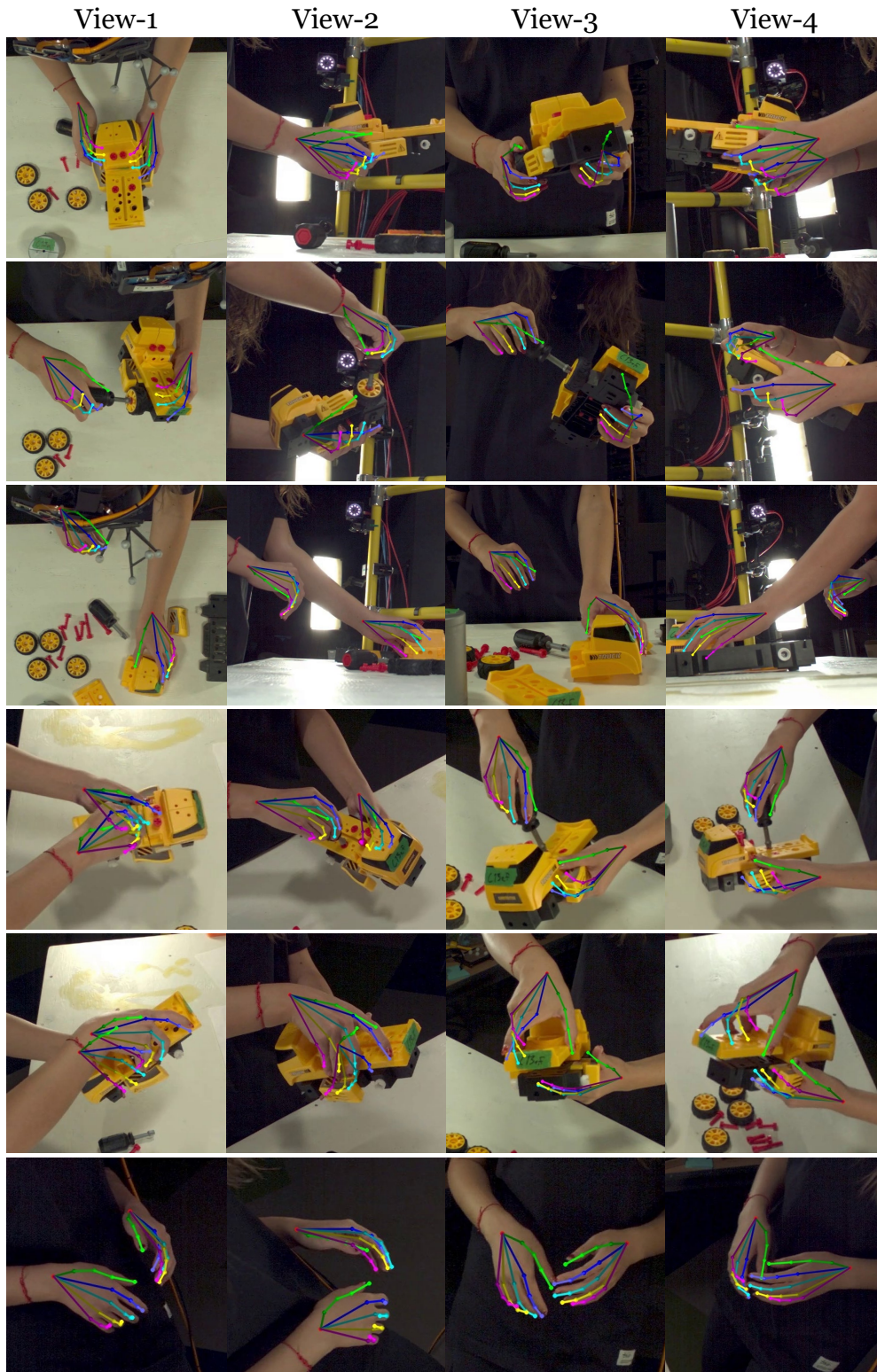


Figure 11. 2D prediction (overlaid in the images) of our method in the testing sequence of the Assembly101 dataset. All the 2D image coordinates are obtained by projecting the same 3D world coordinates into different views. We utilize 8 views in total for inference. Each row shows 4 views of the projected 2D joints. The top 3 rows display the images on 4 views out of all the views, while the bottom 3 rows present the results of another 4 views.

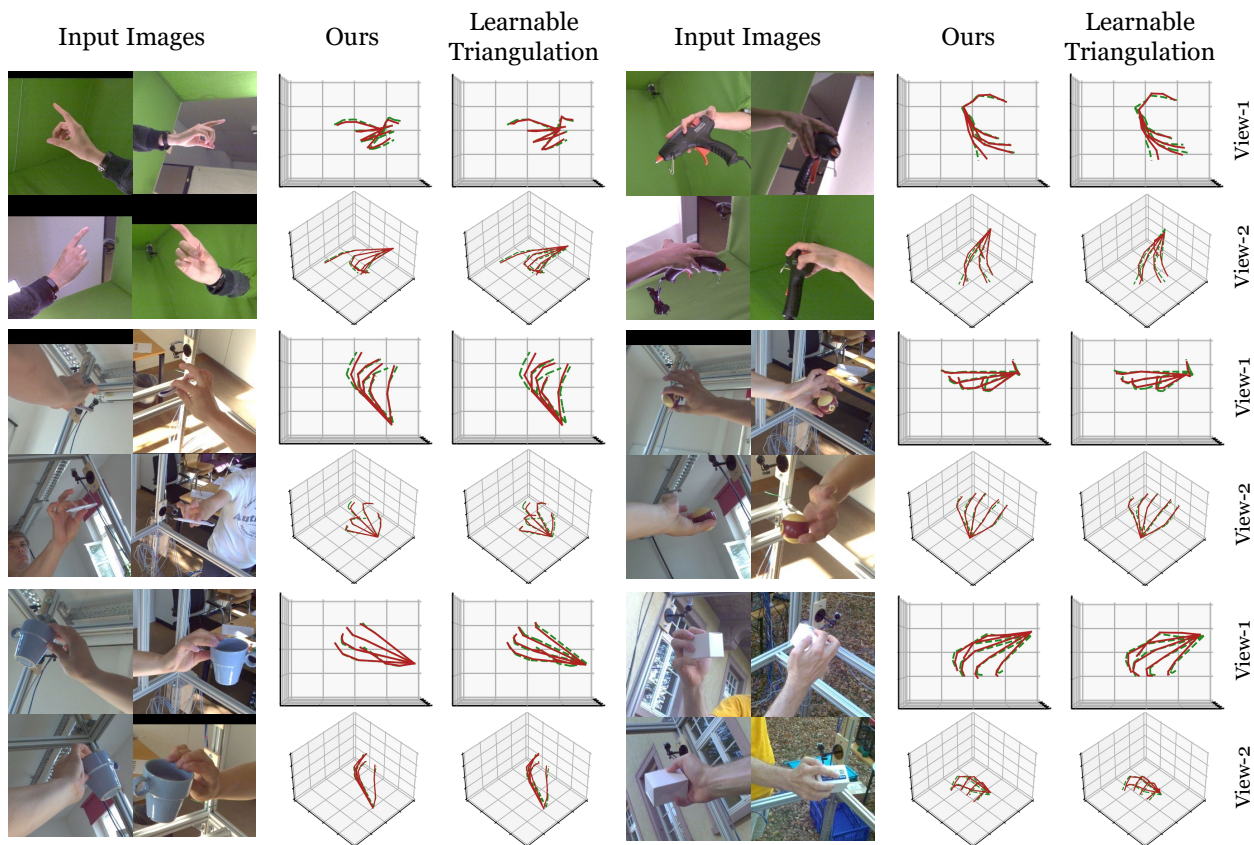


Figure 12. 3D prediction comparisons between our method and Learnable Triangulation on the HanCo dataset. Our prediction and the ground-truth are shown in solid red and dashed green respectively. We use 8 views for inference and only show 4 images here.

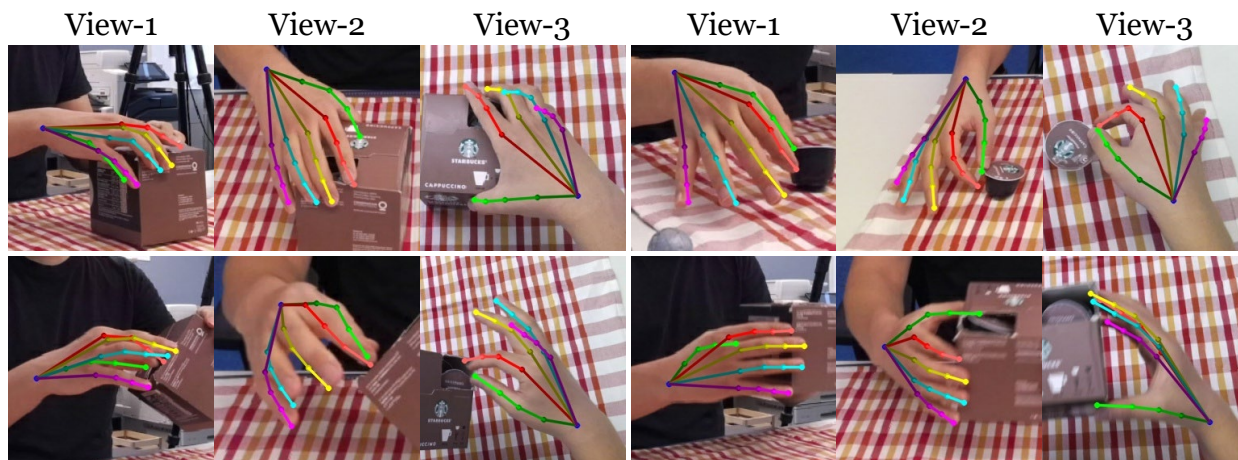


Figure 13. 2D prediction (overlaid in the images) of our method in the testing sequence of the H2O dataset. The results are obtained by the model trained on the HanCo dataset. We use 3 views for inference without camera extrinsics.

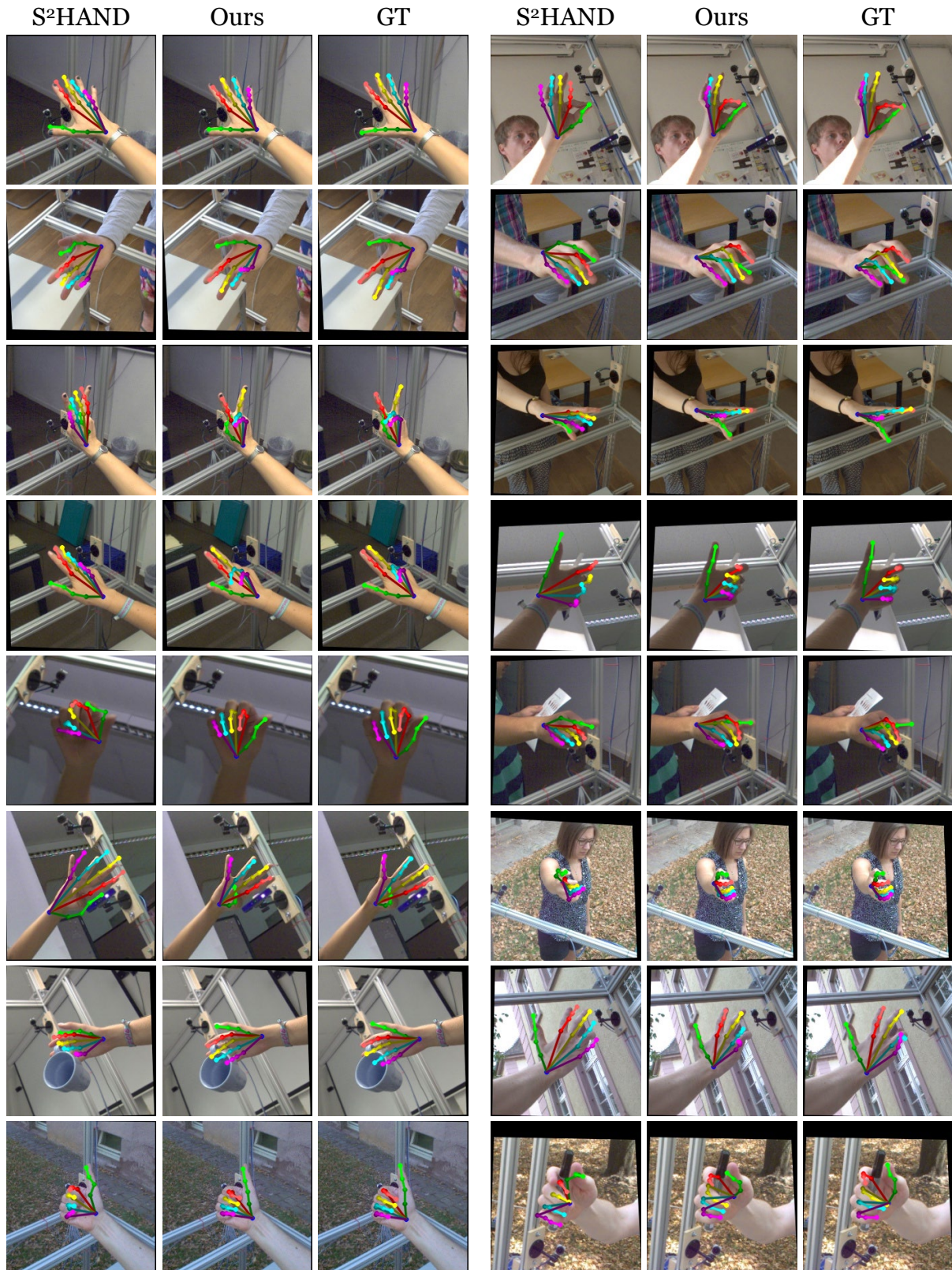


Figure 14. 2D prediction (overlaid in the images) comparisons between S<sup>2</sup>HAND, ours, and the ground-truth on the FreiHAND dataset.



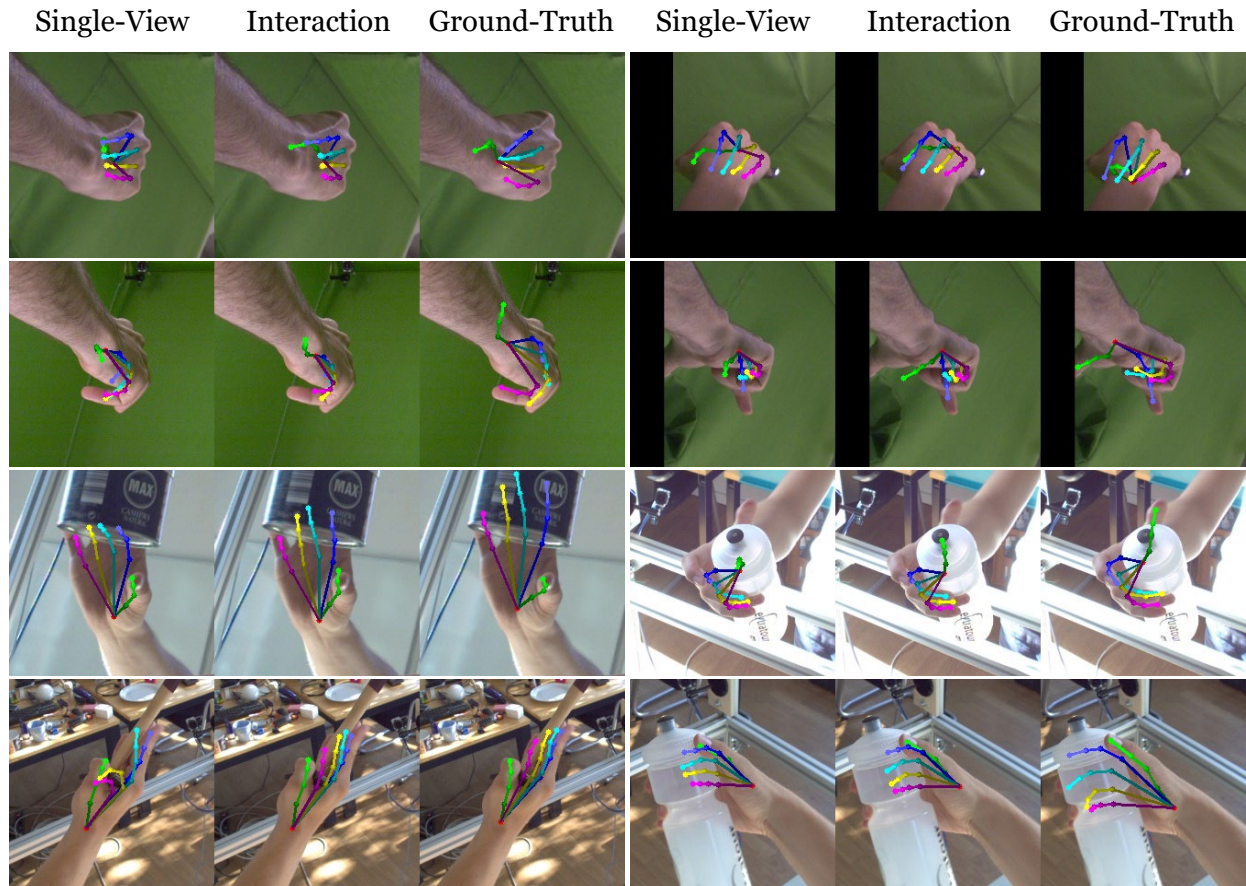


Figure 15. 2D prediction (overlaid in the images) of our failure cases on the HanCo dataset. From left to right, we show our predictions from the single-view network, cross-view interaction network, and the ground-truth.

## References

- [1] Seungryul Baek, Kwang In Kim, and Tae-Kyun Kim. Pushing the envelope for rgb-based dense 3d hand pose estimation via neural rendering. In *Proceedings of the IEEE/CVF Conference on Computer Vision and Pattern Recognition*, pages 1067–1076, 2019. 2, 3
- [2] Seungryul Baek, Kwang In Kim, and Tae-Kyun Kim. Weakly-supervised domain adaptation via gan and mesh model for estimating 3d hand poses interacting objects. In *Proceedings of the IEEE/CVF Conference on Computer Vision and Pattern Recognition*, pages 6121–6131, 2020. 2
- [3] Kristijan Bartol, David Bojanić, Tomislav Petković, and Tomislav Pribanić. Generalizable human pose triangulation. In *Proceedings of the IEEE/CVF Conference on Computer Vision and Pattern Recognition*, pages 11028–11037, 2022. 3
- [4] Adnane Boukhayma, Rodrigo de Bem, and Philip HS Torr. 3d hand shape and pose from images in the wild. In *Proceedings of the IEEE/CVF Conference on Computer Vision and Pattern Recognition*, pages 10843–10852, 2019. 2, 3
- [5] Yujun Cai, Lihao Ge, Jianfei Cai, and Junsong Yuan. Weakly-supervised 3d hand pose estimation from monocular rgb images. In *European Conference on Computer Vision*, pages 666–682, 2018. 2, 3
- [6] Zhe Cao, Tomas Simon, Shih-En Wei, and Yaser Sheikh. Realtime multi-person 2d pose estimation using part affinity fields. In *Proceedings of the IEEE conference on computer vision and pattern recognition*, pages 7291–7299, 2017. 5, 10
- [7] Ping Chen, Yujin Chen, Dong Yang, Fangyin Wu, Qin Li, Qingpei Xia, and Yong Tan. I2uv-handnet: Image-to-uv prediction network for accurate and high-fidelity 3d hand mesh modeling. In *Proceedings of the IEEE/CVF International Conference on Computer Vision*, pages 12929–12938, 2021. 2, 6
- [8] Ting Chen, Simon Kornblith, Mohammad Norouzi, and Geoffrey Hinton. A simple framework for contrastive learning of visual representations. In *International conference on machine learning*, pages 1597–1607. PMLR, 2020. 3
- [9] Xinlei Chen, Haoqi Fan, Ross Girshick, and Kaiming He. Improved baselines with momentum contrastive learning. *arXiv preprint arXiv:2003.04297*, 2020. 3
- [10] Xinlei Chen and Kaiming He. Exploring simple siamese representation learning. In *Proceedings of the IEEE/CVF Conference on Computer Vision and Pattern Recognition*, pages 15750–15758, 2021. 3
- [11] Xingyu Chen, Yufeng Liu, Yajiao Dong, Xiong Zhang, Chongyang Ma, Yanmin Xiong, Yuan Zhang, and Xiaoyan Guo. Mobrecon: Mobile-friendly hand mesh reconstruction from monocular image. In *Proceedings of the IEEE/CVF Conference on Computer Vision and Pattern Recognition*, pages 20544–20554, 2022. 2, 3, 5, 6
- [12] Xingyu Chen, Yufeng Liu, Chongyang Ma, Jianlong Chang, Huayan Wang, Tian Chen, Xiaoyan Guo, Pengfei Wan, and Wen Zheng. Camera-space hand mesh recovery via semantic aggregation and adaptive 2d-1d registration. In *Proceedings of the IEEE/CVF Conference on Computer Vision and Pattern Recognition*, pages 13274–13283, 2021. 2, 3
- [13] Yujin Chen, Zhigang Tu, Di Kang, Linchao Bao, Ying Zhang, Xuefei Zhe, Ruizhi Chen, and Junsong Yuan. Model-based 3d hand reconstruction via self-supervised learning. In *Proceedings of the IEEE/CVF Conference on Computer Vision and Pattern Recognition*, pages 10451–10460, 2021. 1, 2, 3, 6, 11
- [14] Hongsuk Choi, Gyeongsik Moon, and Kyoung Mu Lee. Pose2mesh: Graph convolutional network for 3d human pose and mesh recovery from a 2d human pose. In *European Conference on Computer Vision*, pages 769–787. Springer, 2020. 2
- [15] Jia Deng, Wei Dong, Richard Socher, Li-Jia Li, Kai Li, and Li Fei-Fei. Imagenet: A large-scale hierarchical image database. In *2009 IEEE conference on computer vision and pattern recognition*, pages 248–255. Ieee, 2009. 6
- [16] Junting Dong, Wen Jiang, Qixing Huang, Hujun Bao, and Xiaowei Zhou. Fast and robust multi-person 3d pose estimation from multiple views. In *Proceedings of the IEEE/CVF Conference on Computer Vision and Pattern Recognition*, pages 7792–7801, 2019. 6, 7
- [17] Bardia Doosti, Shujon Naha, Majid Mirbagheri, and David J Crandall. Hope-net: A graph-based model for hand-object pose estimation. In *Proceedings of the IEEE/CVF Conference on Computer Vision and Pattern Recognition*, pages 6608–6617, 2020. 2, 4
- [18] Zicong Fan, Adrian Spurr, Muhammed Kocabas, Siyu Tang, Michael J Black, and Otmar Hilliges. Learning to disambiguate strongly interacting hands via probabilistic per-pixel part segmentation. In *2021 International Conference on 3D Vision (3DV)*, pages 1–10. IEEE, 2021. 2
- [19] Lihao Ge, Hui Liang, Junsong Yuan, and Daniel Thalmann. Robust 3d hand pose estimation in single depth images: from single-view cnn to multi-view cnns. In *Proceedings of the IEEE conference on computer vision and pattern recognition*, pages 3593–3601, 2016. 2
- [20] Lihao Ge, Hui Liang, Junsong Yuan, and Daniel Thalmann. 3d convolutional neural networks for efficient and robust hand pose estimation from single depth images. In *Proceedings of the IEEE conference on computer vision and pattern recognition*, pages 1991–2000, 2017. 2
- [21] Lihao Ge, Zhou Ren, Yuncheng Li, Zehao Xue, Yingying Wang, Jianfei Cai, and Junsong Yuan. 3d hand shape and pose estimation from a single rgb image. In *Proceedings of the IEEE/CVF Conference on Computer Vision and Pattern Recognition*, pages 10833–10842, 2019. 2
- [22] John C Gower. Generalized procrustes analysis. *Psychometrika*, 40(1):33–51, 1975. 6
- [23] Jean-Bastien Grill, Florian Strub, Florent Altché, Corentin Tallec, Pierre Richemond, Elena Buchatskaya, Carl Doersch, Bernardo Avila Pires, Zhaohan Guo, Mohammad Gheshlaghi Azar, et al. Bootstrap your own latent—a new approach to self-supervised learning. *Advances in neural information processing systems*, 33:21271–21284, 2020. 3
- [24] Shreyas Hampali, Mahdi Rad, Markus Oberweger, and Vincent Lepetit. Honnotate: A method for 3d annotation of hand

- and object poses. In *Proceedings of the IEEE/CVF Conference on Computer Vision and Pattern Recognition*, pages 3196–3206, 2020. [2](#)
- [25] Shangchen Han, Beibei Liu, Randi Cabezas, Christopher D Twigg, Peizhao Zhang, Jeff Petkau, Tsz-Ho Yu, Chun-Jung Tai, Muzaffer Akbay, Zheng Wang, et al. Megatrack: monochrome egocentric articulated hand-tracking for virtual reality. *39(4):87–1*, 2020. [1](#)
- [26] Shangchen Han, Po-chen Wu, Yubo Zhang, Beibei Liu, Linguang Zhang, Zheng Wang, Weiguang Si, Peizhao Zhang, Yujun Cai, Tomas Hodan, Cabezas Randi, Tran Luan, Akbay Muzaffer, Yu Tsz-Ho, Keskin Cem, and Wang Robert. Umetrack: Unified multi-view end-to-end hand tracking for vr. *ACM Transactions on Graphics*, 2022. [1](#)
- [27] Richard Hartley and Andrew Zisserman. *Multiple view geometry in computer vision*. Cambridge university press, 2003. [6, 7](#)
- [28] Kaiming He, Haoqi Fan, Yuxin Wu, Saining Xie, and Ross Girshick. Momentum contrast for unsupervised visual representation learning. In *Proceedings of the IEEE/CVF Conference on Computer Vision and Pattern Recognition*, pages 9729–9738, 2020. [3](#)
- [29] Kaiming He, Xiangyu Zhang, Shaoqing Ren, and Jian Sun. Deep residual learning for image recognition. In *Proceedings of the IEEE conference on computer vision and pattern recognition*, pages 770–778, 2016. [6, 9](#)
- [30] Yihui He, Rui Yan, Katerina Fragkiadaki, and Shoou-I Yu. Epipolar transformers. In *Proceedings of the IEEE/CVF conference on computer vision and pattern recognition*, pages 7779–7788, 2020. [3, 6](#)
- [31] Umar Iqbal, Pavlo Molchanov, Thomas Breuel Juergen Gall, and Jan Kautz. Hand pose estimation via latent 2.5 d heatmap regression. In *Proceedings of the European Conference on Computer Vision*, pages 118–134, 2018. [2](#)
- [32] Umar Iqbal, Pavlo Molchanov, and Jan Kautz. Weakly-supervised 3d human pose learning via multi-view images in the wild. In *Proceedings of the IEEE/CVF Conference on Computer Vision and Pattern Recognition*, pages 5243–5252, 2020. [2, 3, 8](#)
- [33] Karim Isakov, Egor Burkov, Victor Lempitsky, and Yury Malkov. Learnable triangulation of human pose. In *Proceedings of the IEEE/CVF International Conference on Computer Vision*, pages 7718–7727, 2019. [3, 6, 7, 11](#)
- [34] Diederik P Kingma and Max Welling. Auto-encoding variational bayes. In *2nd International Conference on Learning Representations*, 2014. [2](#)
- [35] Muhammed Kocabas, Salih Karagoz, and Emre Akbas. Self-supervised learning of 3d human pose using multi-view geometry. In *Proceedings of the IEEE/CVF Conference on Computer Vision and Pattern Recognition*, pages 1077–1086, 2019. [1, 3, 5, 6, 11](#)
- [36] Dominik Kulon, Riza Alp Guler, Iasonas Kokkinos, Michael M Bronstein, and Stefanos Zafeiriou. Weakly-supervised mesh-convolutional hand reconstruction in the wild. In *Proceedings of the IEEE/CVF Conference on Computer Vision and Pattern Recognition*, pages 4990–5000, 2020. [2, 6](#)
- [37] Taemin Kwon, Bugra Tekin, Jan Stühmer, Federica Bogo, and Marc Pollefeys. H2o: Two hands manipulating objects for first person interaction recognition. In *Proceedings of the IEEE/CVF International Conference on Computer Vision*, pages 10138–10148, 2021. [1, 2, 5, 10](#)
- [38] Mengcheng Li, Liang An, Hongwen Zhang, Lianpeng Wu, Feng Chen, Tao Yu, and Yebin Liu. Interacting attention graph for single image two-hand reconstruction. In *Proceedings of the IEEE/CVF Conference on Computer Vision and Pattern Recognition*, pages 2761–2770, 2022. [2, 3](#)
- [39] Moran Li, Yuan Gao, and Nong Sang. Exploiting learnable joint groups for hand pose estimation. In *Proceedings of the AAAI Conference on Artificial Intelligence*, volume 35, pages 1921–1929, 2021. [2](#)
- [40] Kevin Lin, Lijuan Wang, and Zicheng Liu. End-to-end human pose and mesh reconstruction with transformers. In *Proceedings of the IEEE/CVF Conference on Computer Vision and Pattern Recognition*, pages 1954–1963, 2021. [2, 6](#)
- [41] Kevin Lin, Lijuan Wang, and Zicheng Liu. Mesh graphormer. In *Proceedings of the IEEE/CVF International Conference on Computer Vision*, pages 12939–12948, 2021. [2, 3](#)
- [42] Ilya Loshchilov and Frank Hutter. Decoupled weight decay regularization. In *7th International Conference on Learning Representations*, 2019. [6](#)
- [43] Haoyu Ma, Zhe Wang, Yifei Chen, Deying Kong, Liangjian Chen, Xingwei Liu, Xiangyi Yan, Hao Tang, and Xiaohui Xie. Ppt: token-pruned pose transformer for monocular and multi-view human pose estimation. In *European Conference on Computer Vision*, pages 424–442. Springer, 2022. [3](#)
- [44] Gyeongsik Moon, Ju Yong Chang, and Kyoung Mu Lee. V2v-posenet: Voxel-to-voxel prediction network for accurate 3d hand and human pose estimation from a single depth map. In *Proceedings of the IEEE conference on computer vision and pattern Recognition*, pages 5079–5088, 2018. [2](#)
- [45] Gyeongsik Moon and Kyoung Mu Lee. I2l-meshnet: Image-to-lixel prediction network for accurate 3d human pose and mesh estimation from a single rgb image. In *European Conference on Computer Vision*, pages 752–768. Springer, 2020. [2, 6](#)
- [46] Gyeongsik Moon, Shoou-I Yu, He Wen, Takaaki Shiratori, and Kyoung Mu Lee. Interhand2. 6m: A dataset and baseline for 3d interacting hand pose estimation from a single rgb image. In *European Conference on Computer Vision*, pages 548–564. Springer, 2020. [2](#)
- [47] Franziska Mueller, Florian Bernard, Oleksandr Sotnychenko, Dushyant Mehta, Srinath Sridhar, Dan Casas, and Christian Theobalt. Gnerated hands for real-time 3d hand tracking from monocular rgb. In *Proceedings of the IEEE Conference on Computer Vision and Pattern Recognition*, pages 49–59, 2018. [2, 3](#)
- [48] Adam Paszke, Sam Gross, Soumith Chintala, Gregory Chanan, Edward Yang, Zachary DeVito, Zeming Lin, Alban Desmaison, Luca Antiga, and Adam Lerer. Automatic differentiation in pytorch. 2017. [6](#)
- [49] Georgios Pavlakos, Xiaowei Zhou, Konstantinos G Derpanis, and Kostas Daniilidis. Harvesting multiple views for

- marker-less 3d human pose annotations. In *Proceedings of the IEEE conference on computer vision and pattern recognition*, pages 6988–6997, 2017. [3](#)
- [50] Haibo Qiu, Chunyu Wang, Jingdong Wang, Naiyan Wang, and Wenjun Zeng. Cross view fusion for 3d human pose estimation. In *Proceedings of the IEEE/CVF International Conference on Computer Vision*, pages 4342–4351, 2019. [3](#)
- [51] Edoardo Remelli, Shangchen Han, Sina Honari, Pascal Fua, and Robert Wang. Lightweight multi-view 3d pose estimation through camera-disentangled representation. In *Proceedings of the IEEE/CVF Conference on Computer Vision and Pattern Recognition*, pages 6040–6049, 2020. [3](#)
- [52] Helge Rhodin, Jörg Spörrli, Isinsu Katircioglu, Victor Constantin, Frédéric Meyer, Erich Müller, Mathieu Salzmann, and Pascal Fua. Learning monocular 3d human pose estimation from multi-view images. In *Proceedings of the IEEE conference on computer vision and pattern recognition*, pages 8437–8446, 2018. [3](#)
- [53] Javier Romero, Dimitrios Tzionas, and Michael J. Black. Embodied hands: Modeling and capturing hands and bodies together. *ACM Transactions on Graphics*, 36(6), 2017. [2](#), [3](#), [9](#)
- [54] Fadime Sener, Dibiyadip Chatterjee, Daniel Shelepov, Kun He, Dipika Singhania, Robert Wang, and Angela Yao. Assembly101: A large-scale multi-view video dataset for understanding procedural activities. In *Proceedings of the IEEE/CVF Conference on Computer Vision and Pattern Recognition*, pages 21096–21106, 2022. [1](#), [2](#), [5](#), [10](#)
- [55] Hui Shuai, Lele Wu, and Qingshan Liu. Adaptive multi-view and temporal fusing transformer for 3d human pose estimation. *IEEE Transactions on Pattern Analysis and Machine Intelligence*, 2022. [3](#)
- [56] Tomas Simon, Hanbyul Joo, Iain Matthews, and Yaser Sheikh. Hand keypoint detection in single images using multiview bootstrapping. In *Proceedings of the IEEE conference on Computer Vision and Pattern Recognition*, pages 1145–1153, 2017. [10](#)
- [57] Adrian Spurr, Aneesh Dahiya, Xi Wang, Xucong Zhang, and Otmar Hilliges. Self-supervised 3d hand pose estimation from monocular rgb via contrastive learning. In *Proceedings of the IEEE/CVF International Conference on Computer Vision*, pages 11230–11239, 2021. [3](#)
- [58] Adrian Spurr, Umar Iqbal, Pavlo Molchanov, Otmar Hilliges, and Jan Kautz. Weakly supervised 3d hand pose estimation via biomechanical constraints. In *European Conference on Computer Vision*, pages 211–228. Springer, 2020. [2](#), [3](#)
- [59] Adrian Spurr, Jie Song, Seonwook Park, and Otmar Hilliges. Cross-modal deep variational hand pose estimation. In *Proceedings of the IEEE conference on computer vision and pattern recognition*, pages 89–98, 2018. [2](#)
- [60] Xiao Tang, Tianyu Wang, and Chi-Wing Fu. Towards accurate alignment in real-time 3d hand-mesh reconstruction. In *Proceedings of the IEEE/CVF International Conference on Computer Vision*, pages 11698–11707, 2021. [2](#), [6](#)
- [61] Hanyue Tu, Chunyu Wang, and Wenjun Zeng. Voxelpose: Towards multi-camera 3d human pose estimation in wild environment. In *European Conference on Computer Vision*, pages 197–212. Springer, 2020. [3](#)
- [62] Bastian Wandt, Marco Rudolph, Petrisa Zell, Helge Rhodin, and Bodo Rosenhahn. Canonpose: Self-supervised monocular 3d human pose estimation in the wild. In *Proceedings of the IEEE/CVF Conference on Computer Vision and Pattern Recognition*, pages 13294–13304, 2021. [1](#), [3](#), [5](#), [6](#), [11](#)
- [63] Nanyang Wang, Yinda Zhang, Zhuwen Li, Yanwei Fu, Wei Liu, and Yu-Gang Jiang. Pixel2mesh: Generating 3d mesh models from single rgb images. In *European Conference on Computer Vision*, pages 52–67. Springer, 2018. [4](#), [9](#)
- [64] Chao Wen, Yinda Zhang, Zhuwen Li, and Yanwei Fu. Pixel2mesh++: Multi-view 3d mesh generation via deformation. In *Proceedings of the IEEE/CVF international conference on computer vision*, pages 1042–1051, 2019. [4](#), [9](#)
- [65] Linlin Yang, Shicheng Chen, and Angela Yao. Semihand: Semi-supervised hand pose estimation with consistency. In *Proceedings of the IEEE/CVF International Conference on Computer Vision*, pages 11364–11373, 2021. [2](#), [3](#)
- [66] Linlin Yang, Shile Li, Dongheui Lee, and Angela Yao. Aligning latent spaces for 3d hand pose estimation. In *Proceedings of the IEEE/CVF International Conference on Computer Vision*, pages 2335–2343, 2019. [2](#)
- [67] Linlin Yang and Angela Yao. Disentangling latent hands for image synthesis and pose estimation. In *Proceedings of the IEEE/CVF Conference on Computer Vision and Pattern Recognition*, pages 9877–9886, 2019. [2](#)
- [68] Xiong Zhang, Hongsheng Huang, Jianchao Tan, Hongmin Xu, Cheng Yang, Guozhu Peng, Lei Wang, and Ji Liu. Hand image understanding via deep multi-task learning. In *Proceedings of the IEEE/CVF International Conference on Computer Vision*, pages 11281–11292, 2021. [2](#)
- [69] Xiong Zhang, Qiang Li, Hong Mo, Wenbo Zhang, and Wen Zheng. End-to-end hand mesh recovery from a monocular rgb image. In *Proceedings of the IEEE/CVF International Conference on Computer Vision*, pages 2354–2364, 2019. [2](#), [3](#)
- [70] Zhe Zhang, Chunyu Wang, Weichao Qiu, Wenhui Qin, and Wenjun Zeng. Adafuse: Adaptive multiview fusion for accurate human pose estimation in the wild. *International Journal of Computer Vision*, 129(3):703–718, 2021. [3](#)
- [71] Xiaozheng Zheng, Pengfei Ren, Haifeng Sun, Jingyu Wang, Qi Qi, and Jianxin Liao. Sar: Spatial-aware regression for 3d hand pose and mesh reconstruction from a monocular rgb image. In *2021 IEEE International Symposium on Mixed and Augmented Reality*, pages 99–108, 2021. [2](#), [3](#), [4](#), [9](#)
- [72] Christian Zimmermann, Max Argus, and Thomas Brox. Contrastive representation learning for hand shape estimation. In *DAGM German Conference on Pattern Recognition*, pages 250–264. Springer, 2021. [1](#), [2](#), [3](#), [5](#), [7](#), [10](#)
- [73] Christian Zimmermann and Thomas Brox. Learning to estimate 3d hand pose from single rgb images. In *Proceedings of the IEEE international conference on computer vision*, pages 4903–4911, 2017. [2](#), [3](#)
- [74] Christian Zimmermann, Duygu Ceylan, Jimei Yang, Bryan Russell, Max Argus, and Thomas Brox. Freihand: A dataset for markerless capture of hand pose and shape from single rgb images. In *Proceedings of the IEEE/CVF International Conference on Computer Vision*, pages 813–822, 2019. [1](#), [2](#), [5](#), [11](#)